IMPACT OF CRYSTALLIZATION FOULING ON THE MOISTURE TRANSFER RESISTANCE OF A LIQUID-TO-AIR MEMBRANE ENERGY EXCHANGER

A.O. Olufade[1] and C.J. Simonson[1]

[1] Department of Mechanical Engineering, University of Saskatchewan, 57 Campus Dr., Saskatoon, SK S7N 5A9, Canada, aoo021@mail.usask.ca

ABSTRACT

Liquid-to-air membrane energy exchangers (LAMEEs) use membranes to exchange heat and moisture between liquid and air streams while preventing direct contact between the fluids. Furthermore, LAMEEs are energy-efficient and environmentally friendly, and have potential application in air-conditioning systems. The performance of LAMEEs may, however, be significantly compromised if crystallization fouling occurs within the membrane.

The main aims of this study are to detect crystallization fouling in a LAMEE, and to evaluate the impact of fouling on the moisture transfer resistance of a LAMEE. Experimental tests are performed on a LAMEE using supersaturated $MgCl_2$(aq) solution and distilled water.

A statistical method is used to analyze the test data. The results indicate that crystallization fouling can be detected in a LAMEE in less than 5 hours. In addition, crystallization fouling can increase the resistance of a LAMEE by over a factor of 2.

INTRODUCTION

Fouling involves the formation, accumulation and attachment of unwanted matter on a surface (Field, 2010). Fouling deposits can attach to the surface of a heat exchanger or a membrane. Heat exchanger fouling reduces the overall heat transfer coefficient of heat exchangers (Geddert et al., 2011), whereas membrane fouling limits the effective transport of fluid through the pores of membranes (Field, 2010). Consequently, fouling increases operational and productions costs in industries due to additional power consumption, heat exchanger oversizing, material consumption and maintenance (Müller-Steinhagen, 2011; Guo et al., 2012). The economic cost of heat exchanger fouling to developed countries is up to 0.25% of the gross domestic product (Müller-Steinhagen, 2011), which is roughly equal to US$ 4 billion for Canada in 2015, based on information from The World Bank Group (The World Bank Group, 2016).

This paper addresses fouling in heating, ventilation and air-conditioning (HVAC) applications. This is because HVAC systems account for almost 20% of the energy consumed in developed nations (Pérez-Lombard et al., 2008). Furthermore, HVAC systems account for over half of the energy consumed in residential and commercial/institutional buildings in Canada (National Resources Canada, 2015). Obviously, HVAC systems play a significant role towards achieving energy efficiency and sustainability, especially in buildings where most people spend over 80% of their time (Yu et al., 2009).

This paper specifically focuses on fouling in membrane exchangers, which are a recent development for HVAC applications. Fouling studies on HVAC applications are generally limited to heat exchangers (Wright et al., 2009; Shen et al., 2015), and the mechanisms of fouling in membrane exchangers are not well-understood (Woods, 2014).

So far, only two studies on fouling in membrane-based HVAC applications have been found in the literature. The studies of Charles and Johnson (2008) and Crawford and da Silva (2014) experimentally assessed the impact of crystallization fouling on the performance of membrane evaporative cooling units, and found that fouling could reduce the rate of moisture transfer through a membrane by over 90%. However, these two studies neither considered liquid desiccants nor characterized the impact of fouling on the moisture transfer resistance of the exchangers tested.

This paper aims to address the aforementioned gaps on fouling in membrane-based energy exchangers for HVAC applications. The specific objectives of this paper are to: i) detect crystallization fouling in a LAMEE, ii) assess the impact of crystallization fouling on the moisture transfer resistance of a LAMEE, and iii) evaluate the effect of the rate of moisture transfer through a membrane on crystallization fouling in a LAMEE.

THEORETICAL BACKGROUND

Crystallization Mechanisms

Crystallization fouling involves the precipitation of ions from a salt solution or suspended particles in a bulk liquid, and subsequent attachment to a surface (Bott, 1997). There are several factors that affect crystallization fouling, including fluid properties (concentration, pH), surface properties (defects, roughness) and operating conditions (temperature, velocity) (Walker and Sheikholeslami, 2003; Pääkkönen et al., 2012). Nevertheless, supersaturation is a key requirement for the occurrence of crystallization (Mullin, 2001; Walker and Sheikholeslami, 2003).

Supersaturation can be achieved through evaporating a salt solution above its solubility, cooling a normal solubility

ISBN: 978-0-9984188-0-3; Published online www.heatexchanger-fouling.com

salt solution below its saturation temperature, or heating a reverse solubility salt solution above its saturation temperature (Bansal et al., 2008).

Once supersaturation is attained, surface defects and suspended particles in the liquid may initiate the seeding of crystals (Bott, 1997). Crystals may nucleate on a surface (surface crystallization), or within the bulk solution (bulk crystallization) and deposit on the surface of a heat exchanger or membrane (Bott, 1997; Tijing et al., 2015). Nucleation is succeeded by crystal growth as crystals begin to accumulate and grow on a surface (Mullin, 2001).

Crystallization Fouling in a LAMEE

A schematic diagram of a LAMEE without and with fouling is shown in Fig. 1.

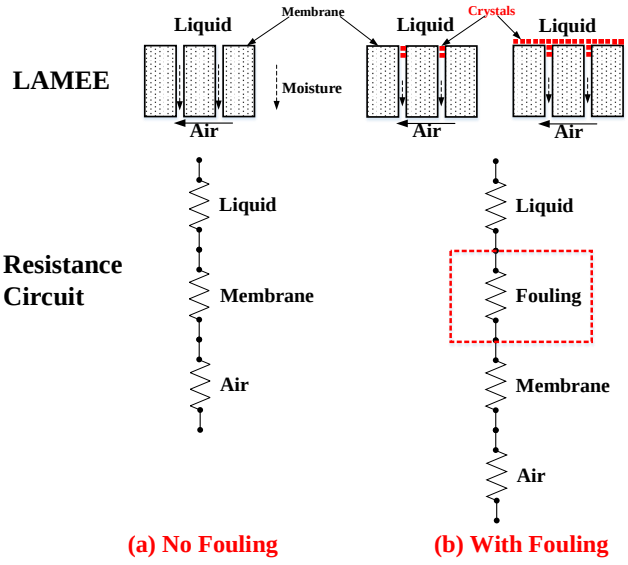

Fig. 1 Schematic diagram of a LAMEE and its constituent resistances (a) without and (b) with fouling.

Fig. 1 shows a simplified schematic of the LAMEE, which essentially consists of an air stream and a stagnant liquid desiccant, which are separated by a semi-permeable membrane. As air flows on one side of the membrane, moisture evaporates from the liquid desiccant and permeates through the membrane pores to the air side (Fig. 1a). If the evaporation rate is high, the interface or bulk solution concentration will increase until it reaches supersaturation, and crystals may begin to nucleate and block the pores of the membrane. Crystal formation may continue until a cake layer is formed on the surface of the membrane (Fig. 1b).

Fig. 1 also shows the constituent resistances of a LAMEE without and with the occurrence of fouling. The resistance of the LAMEE consists of the liquid-side, membrane and air-side resistances if there is no fouling (Fig. 1a). An additional resistance (fouling resistance) is added to the resistance of the LAMEE if fouling occurs (Fig. 1b). The fouling resistance is caused by the formation of crystals which impede moisture transfer through the membrane.

The impact of fouling on the resistance of a LAMEE can be evaluated by comparing the resistance of the LAMEE without and with fouling. Consequently, the occurrence of fouling during a test is expected to increase the magnitude of resistance of the LAMEE. However, the resistance of an exchanger does not only increase in magnitude when fouling occurs, but also exhibits distinct trends depending on the underlying deposit formation processes. A number of fouling resistance trends for heat exchangers are shown in Fig. 2.

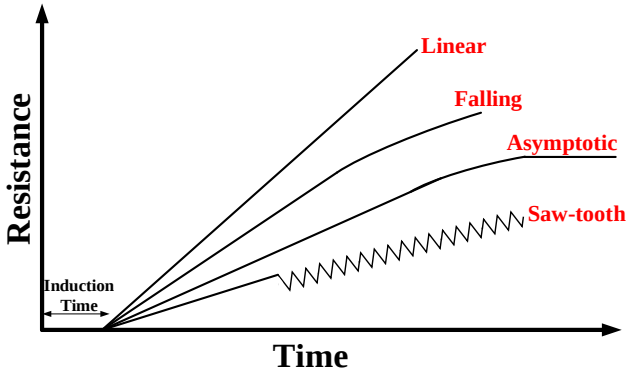

Fig. 2 Trends of fouling resistance in heat exchangers, as adapted from Bansal et al. (2008) and Müller-Steinhagen (2011).

The trends in the fouling resistances shown in Fig. 2 are briefly explained based on Bansal et al. (2008) and Müller-Steinhagen (2011). Fouling typically results in the deposition and possible removal of particles from the surface of a heat exchanger. Fouling resistance exhibits a linear trend if the deposition rate of particles is substantially higher than the removal rate, provided that the removal rate is fixed or insignificant. A falling fouling trend occurs if the deposits are not tenacious and their removal rate increases over time. Asymptotic fouling occurs when the deposits are weakly attached to a surface, such that the removal rate of particles increases over time until it equals the deposition rate. Finally, a saw-tooth fouling trend occurs when the particles that attach to a surface continually shear off and are re-attached.

EXPERIMENT

Test Facility

A test facility is constructed to test the LAMEE at operating conditions that simulate crystallization fouling. As previously explained, the LAMEE enables the exchange of heat and moisture between an air stream and a stagnant liquid desiccant solution through a semi-permeable membrane. The continuous evaporation of moisture from the desiccant solution may increase the bulk or interfacial solution concentration to supersaturation conditions. Once supersaturation is attained, crystals may nucleate directly on the membrane surface or transported from the bulk fluid to the membrane surface.

A schematic diagram of the test facility and LAMEE are shown in Fig. 3(a), and the legend of their components are shown in Fig. 3(b).

ISBN: 978-0-9984188-0-3; Published online www.heatexchanger-fouling.com

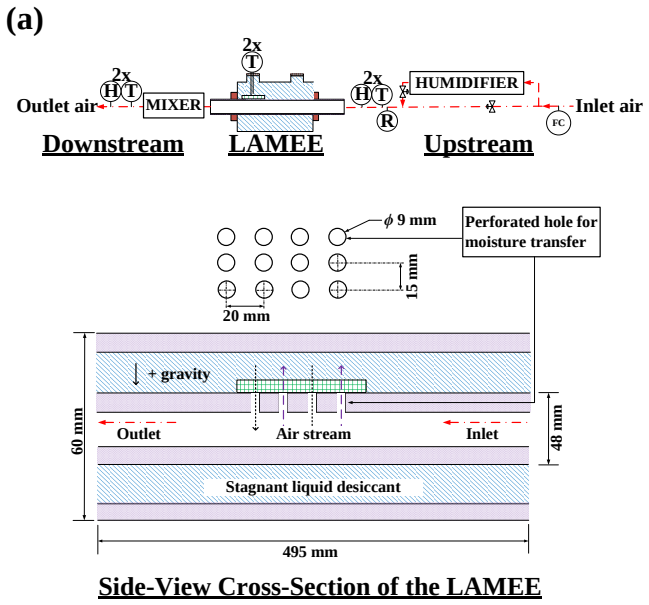

Fig. 3 Schematic of the (a) test facility and (b) legend of the components shown in (a).

In the test section upstream of the LAMEE, a stream of hydro-dynamically fully developed laminar air flow is provided to the inner pipe of the LAMEE. The flow rate of the air stream is controlled with an air flow controller, while its humidity is conditioned with a humidifier. Air is delivered to the LAMEE at a nominal flow rate of 1.4×10^{-5} kg/s via a pipe with an internal diameter (D_h) of 40 mm and an approximate length of 1000 mm ($\approx 25 \cdot D_h$).

The LAMEE is a double-pipe energy exchanger and is made up of inner and outer pipes. The inner pipe is the channel for air flow whereas the outer pipe holds the desiccant solution. Twelve holes are perforated on the inner pipe because the pipe is impermeable to moisture transfer. Consequently, the holes are the areas that permit moisture transfer between the air stream and desiccant solution through the membrane.

The air stream that exits the LAMEE is mixed to achieve uniform properties in the test section downstream of the LAMEE. The temperature and relative humidity of air at the inlet and outlet of the LAMEE are recorded with thermocouples and capacitance-based humidity sensors, respectively. The acquisition and measurement of the test data is performed using hardware and software from National Instruments.

The membrane used in the LAMEE is made from expanded polytetrafluoroethylene (ePTFE), and its specifications are given in Tab. 1.

Table 1 Specifications of the membrane used in the LAMEE (Beriault, 2011).

Parameter and unit	Value
Pore size [μm]	0.3
Porosity [%]	85
Vapor diffusion resistance [s/m]	97 ± 11
Water vapor permeability [kg/m·s]	$6.63 \times 10^{-6} \pm 7.7 \times 10^{-7}$
Thickness [mm]	0.54 ± 0.016
Liquid penetration pressure [kPa]	>82

Test Procedure

A membrane is placed over the holes on the inner pipe of the LAMEE using double-sided and aluminum tapes. This enables the membrane to serve as the pathway for moisture transfer between the fluids in the inner and outer pipes of the LAMEE. The air flow system is switched on and a humidifier controls the air humidity to a desired set point. At this stage, the inner pipe of the LAMEE is assembled while the outer pipe remains disassembled. A continuous stream of air is delivered to the inner pipe of the LAMEE to make certain that identical temperature and relative humidity are measured at the upstream and downstream sections of the test facility.

The LAMEE is completely assembled by incorporating both the outer and inner pipes to make a whole exchanger. After assembling the LAMEE, the outer pipe is filled with a liquid desiccant. The data acquisition system is turned on to record the test data. A number of measurements are made during a test, such as the flow rate of air, and the temperature and relative humidity of air at the inlet and outlet of the LAMEE. These measurements are used to calculate the evaporation rate through a membrane and the resistance of the LAMEE.

Furthermore, the mass of the LAMEE is measured both before and after a test with a mass balance, and the density of the liquid desiccant is also measured before and after a test with a density meter. The difference between the initial and final masses of the LAMEE gives an estimate of the quantity of moisture evaporated from the liquid desiccant, whereas the difference between the initial and final density of the liquid desiccant gives an estimate of the change in the bulk concentration of the desiccant solution. The density of the desiccant solution is converted to concentration using a correlation in the literature (Zaytsev and Aseyev, 1992).

The specifications of the instrumentation used for experimental tests are given in Tab. 2.

ISBN: 978-0-9984188-0-3; Published online www.heatexchanger-fouling.com

Table 2. Instrumentation specifications.

Instrument	Parameter (Capacity)	Uncertainty (±)
Thermocouples (T-type)	Temperature (20 °C – 30 °C)	0.2 – 0.3 °C
Humidity sensors (Honeywell HIH)	Relative humidity (10% – 50% RH, 20 °C – 30 °C)	1% RH
Flow controller (MKS 1259C-10000SV)	Flow rate (0.17 L/s)	1%
Rotameter (Dwyer RMB-SSV)	Flow rate (0.04 L/s)	0.001 L/s
Density meter (Anton Paar DMA 4500M)	Density (0 – 3000 kg/m^3)	0.05 kg/m^3
Mass balance (OHAUS Voyager Pro VP6102CN)	Mass (6.1 kg)	0.00109 kg

Note. The uncertainty in the area of the membrane is assumed to be 5%.

Moisture and Energy Balances

Moisture and energy balance analyses are performed in order to assess if the experiments conserve both moisture and energy within the measured uncertainty. Moisture and energy balances are evaluated for the LAMEE as follows:

$$MB = \left| \left(m_{LAMEE,i} - m_{LAMEE,f} \right) - \sum_{0}^{t} \dot{m}_{air} \left(W_{air,out} - W_{air,in} \right) \Delta t \right| \leq U_{MB} \quad (1)$$

$$EB = \left| \left(m_{LAMEE,i} - m_{LAMEE,f} \right) h_{fg} - \sum_{0}^{t} \dot{m}_{air} \left(h_{air,out} - h_{air,in} \right) \Delta t \right| \leq U_{EB} \quad (2)$$

The moisture balance in Eq. (1) compares the quantity of moisture evaporated from the stagnant liquid to the quantity of moisture gained by the air stream, whereas the energy balance in Eq. (2) compares the amount of energy exchanged between the liquid and air sides.

A test is conducted to assess the moisture and energy balance of the LAMEE. Distilled water is used in place of a liquid desiccant because of its higher equilibrium relative humidity which creates a greater potential for moisture transfer to the air stream. The results of the moisture and energy balances for the LAMEE is given in Tab. 3.

Table 3. Comparison of moisture and energy balances for the LAMEE, with distilled water at 23 °C and air at 23 °C and 10% RH.

Moisture		Energy	
MB [g]	0.3	EB [kJ]	0.4
U_{MB} [g]	5.2	U_{EB} [kJ]	13.9
$\frac{MB}{m_{v,sol}}$ [%]	10.0	$\frac{EB}{q_{sol}}$ [%]	4.9

Tab. 3 shows that the moisture and energy balances are within their uncertainties. Thus, both moisture and energy are conserved in the experiment.

DATA ANALYSIS

Characterization of Moisture Transfer Resistance

The moisture transfer resistance of the LAMEE is normalized as R* [-], which is given by:

$$R^* = \frac{R}{R_o} \quad (3)$$

R [m^2 s/kg$_a$] is the instantaneous resistance of the LAMEE at any point in a test, whereas R_o [m^2 s/kg$_a$] is the resistance of the LAMEE at the start of a test.

The resistance of the LAMEE, R [m^2 s/kg$_a$], is given by:

$$R = \frac{\Delta W_{lm}}{\dot{m}''_v} \quad (4)$$

The log-mean humidity ratio ΔW_{lm} [kg$_v$/kg$_a$], and moisture transfer flux, $\dot{m}''_v$ [g$_v$/m^2·hour], are given by:

$$\Delta W_{lm} = \frac{\left(W_{sol} - W_{air,in} \right) - \left(W_{sol} - W_{air,out} \right)}{\ln \left(\frac{W_{sol} - W_{air,in}}{W_{sol} - W_{air,out}} \right)} \quad (5)$$

$$\dot{m}''_v = \frac{\dot{m}_{air} \left(W_{air,out} - W_{air,in} \right)}{A_{mem}} \quad (6)$$

Experimental tests are performed at room temperature conditions, using a $MgCl_2$(aq) solution and air at 10% RH. The concentration of the solution is slightly supersaturated (C_{sol}* = 1.03), where C_{sol}* [-] is the ratio of the solution concentration to its saturation concentration at the same temperature. A supersaturated solution is used in order to increase the likelihood of crystallization fouling. The resistance of the LAMEE at the tested operating condition is shown in Fig. 4.

ISBN: 978-0-9984188-0-3; Published online www.heatexchanger-fouling.com

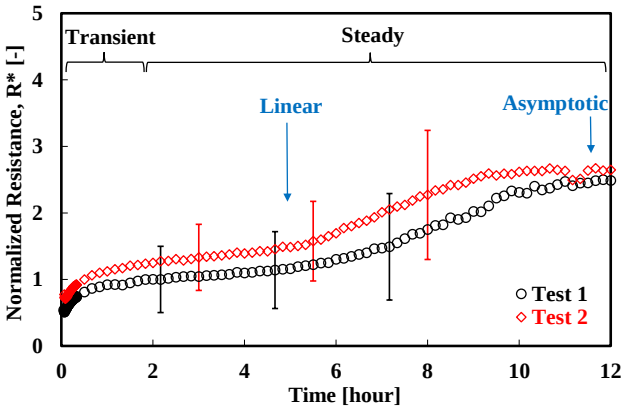

Fig. 4 Normalized resistance as a function of time with $MgCl_2$(aq) at 10% RH, C_{sol}* = 1.03.

There is negligible moisture transfer between the liquid and air sides at the start of the test in Fig. 4. However, as air flows in the inner pipe of the LAMEE, evaporation occurs in the liquid desiccant which is contained in the outer pipe. The transport of water vapor from the desiccant solution through the membrane to the air stream leads to a gradual increase in the resistance of the LAMEE. The increase in the resistance of the LAMEE at the start of the test is primarily due to the higher convective moisture resistance in the air side compared to the desiccant solution, which has a lower moisture transfer resistance.

Nevertheless, the boundary conditions at the air and solution sides are first at transient conditions at the start of the test until they reach steady state. It is important to note that the resistance of the LAMEE continues to increase even after the boundary conditions are at steady state. This is possibly due to the formation of crystals within the membrane, which restrict the rate of moisture transfer through the membrane.

Furthermore, Fig. 4 shows that the resistance of the LAMEE is initially linear in the steady state period, which suggests that crystals may have been deposited on the membrane surface at a continuous rate, and with a negligible removal rate of deposits from the membrane surface. However, the resistance gradually reduces until it reaches an asymptotic point towards the end of the test, such that the deposition and removal rate of crystals from the membrane surface are probably the same. Although the results in Fig. 4 strongly suggest the occurrence of fouling, a definite conclusion cannot be made at this point.

The repeatability of the experiment is also assessed in Fig. 4, which compares two tests at the same operating condition. The experiment is repeatable since the resistances in the two tests are within their uncertainty bounds, and their values closely converge to the same magnitude (~2.5 – 2.7) in the asymptotic period of the tests.

The total uncertainty (U) in resistance combines the systematic (B) and random (P) uncertainties in order to maintain 95% confidence intervals according to ASME PTC Standard 19.1 (ASME/ANSI, 1998):

$$U = \sqrt{B^2 + P^2} \tag{7}$$

The systematic uncertainty in resistance is calculated from the uncertainties propagated in the constituent variables, and is mathematically expressed by Figliola and Beasley (2006):

$$B = \sqrt{\sum_{n=1}^{n_{max}} \left(\frac{\partial R^*}{\partial \varphi_n} B\varphi_n \right)^2} \tag{8}$$

The random uncertainty is calculated by fitting the data to a trend line (linear period in Fig. 4), and multiplying the Student distribution constant (t') with the Standard Error of Estimate (SEE):

$$P = t' \cdot SEE \tag{9}$$

Detection of Crystallization Fouling

A statistical method is used to detect crystallization fouling in the LAMEE, as adapted from Kim et al. (2016). The statistical method uses a hypothesis test to confirm or reject the occurrence of fouling in a test, and to determine the time of fouling whenever fouling is confirmed for a test.

The occurrence of fouling is examined by comparing a hypothetical scenario where there is no fouling (Group 1) with a test where fouling is investigated (Group 2). Thus, Group 1 serves as the control group whereas Group 2 represents the actual test data under evaluation. The occurrence of fouling is thereby confirmed when there is a statistically significant difference between the means of Groups 1 and 2, and rejected when there is a statistically insignificant difference between the means of Groups 1 and 2. The populations of Groups 1 and 2 for a test are shown in Fig. 5.

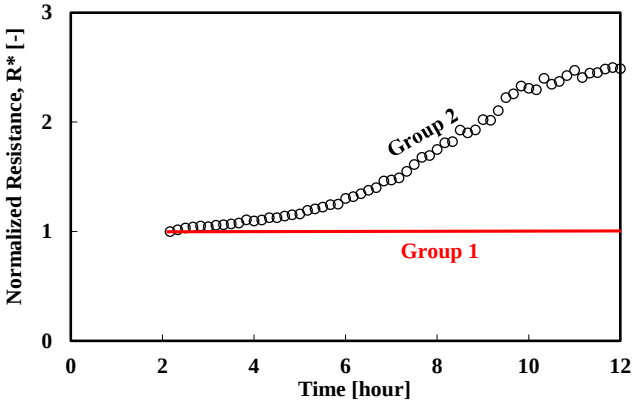

Fig. 5 Normalized resistance as a function of time for a test with $MgCl_2$(aq) at 10% RH, C_{sol}* = 1.03. Groups 1 and 2 are indicated in Fig. 5.

Group 1 consists of the resistance of the LAMEE at the start of the test (i.e. R* = 1) when there is no fouling. The standard deviation of Group 1 is set at ±5%, which represents the maximum deviation in the resistance of the LAMEE for experiments performed using distilled water. The standard deviation of Group 1 stands for the random error in the resistance of the LAMEE at 95% confidence for a test

without fouling. Group 2 consists of the resistance of the LAMEE during an entire test, and its standard deviation is calculated from the test data.

First of all, the statistical method is used to compare Groups 1 and 2 in order to investigate the occurrence of fouling during a test. Afterwards, a moving window is implemented for Groups 1 and 2 in order to conclude the time that fouling occurs. A t-test is used to compare Groups 1 and 2 based on the following null hypothesis:

$$\overline{R_{Group\ 1}} - \overline{R_{Group\ 2}} = d = \left|\sigma_{R_{Group\ 1}} - \sigma_{R_{Group\ 2}}\right| \tag{10}$$

The null hypothesis for the t-test in Eq. (10) states that difference between the means of Groups 1 and 2 is equivalent to the difference in their standard deviations (d). Consequently, the null hypothesis is rejected if the absolute value of the t-test is greater than the critical t-value at 95% confidence and corresponding degrees of freedom, as given by:

$$f = \left(\left|t_{1\text{-}2}\right| - t_{df,95\%}\right) > 0 \tag{11}$$

The null hypothesis is, however, accepted if the fouling detection parameter (f) does not satisfy the condition in Eq. (11). Thus, the occurrence of fouling is statistically established when the null hypothesis is rejected, whereas fouling is deemed to be absent when the null hypothesis is accepted.

The t-statistic ($t_{1\text{-}2}$) and degrees of freedom (df) are calculated using the following equations (Stamatis, 2012):

$$t_{1\text{-}2} = \frac{\left(\overline{R_{Group\ 1}} - \overline{R_{Group\ 2}}\right) - d}{\sqrt{\frac{\sigma^2_{R,\,Group\ 1}}{n_{Group\ 1}} + \frac{\sigma^2_{R,\,Group\ 2}}{n_{Group\ 2}}}} \tag{12}$$

$$df = \frac{\left(\frac{\sigma^2_{R,\,Group\ 1}}{n_{Group\ 1}} + \frac{\sigma^2_{R,\,Group\ 2}}{n_{Group\ 2}}\right)^2}{\frac{\left(\frac{\sigma^2_{R,\,Group\ 1}}{n_{Group\ 1}}\right)^2}{n_{Group\ 1} - 1} + \frac{\left(\frac{\sigma^2_{R,\,Group\ 2}}{n_{Group\ 2}}\right)^2}{n_{Group\ 2} - 1}} \tag{13}$$

The results of the statistical analysis is shown in Fig. 6.

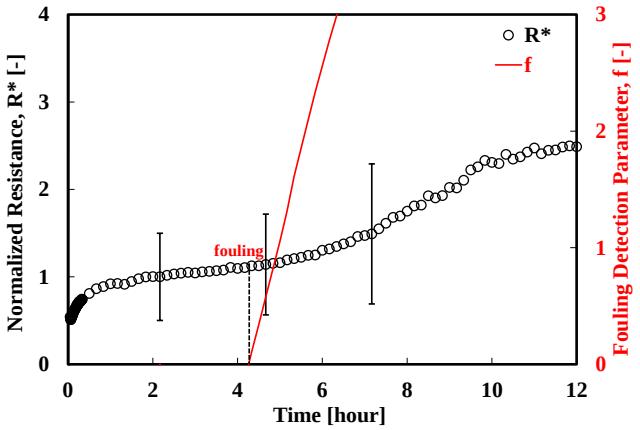

Fig. 6 Normalized resistance and fouling detection parameter as a function of time for a test with $MgCl_2$(aq) at 10% RH of air, C_{sol}* = 1.03.

Fig 6 shows the evolution of resistance of the LAMEE and fouling detection parameter during a test with supersaturated $MgCl_2$(aq). The fouling detection parameter exceeds the value of 0 and satisfies Eq. (11). It can therefore be concluded that crystallization fouling is detected during the test within ~4.3 hours.

RESULTS AND DISCUSSION

Impact of Fouling on the Resistance of a LAMEE

The impact of crystallization fouling on the resistance of a LAMEE is assessed by comparing the resistances of the LAMEE using a supersaturated $MgCl_2$(aq)solution versus distilled water, as shown in Fig. 7.

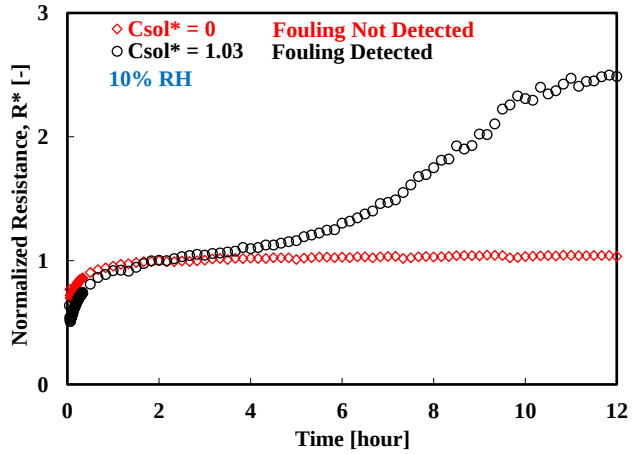

Fig. 7 Comparison of normalized resistance for tests with $MgCl_2$(aq) (C_{sol}* = 1.03) versus distilled water (C_{sol}* = 0) at 10% RH of air.

Fig. 7 shows that the resistance of the LAMEE for distilled water (C_{sol}* = 0) increases at the start of the test when the boundary conditions are transient until it reaches a value of 1. Thereafter, the resistance remains flat for the entire duration of the test. Obviously, there is no fouling during the test with distilled water since the resistance of the LAMEE maintains a constant value of 1.

However, fouling is detected during the test with a supersaturated solution (C_{sol}* = 1.03). This explains the rapid increase in the resistance of the LAMEE during the test. In addition, the supersaturated state of the desiccant solution at the start of the test increases the possibility of spontaneous crystallization within the bulk solution. There is also a possibility that the high rate of evaporation in the desiccant solution may initiate nucleation on the surface of the membrane. Thus, the rapid seeding of crystals within the desiccant solution and at the membrane interface may have blocked the membrane pores and result in a substantial increase in the resistance of the LAMEE.

Impact of Moisture Transfer Rate on Fouling in a LAMEE

An objective of this paper is to assess the impact of the rate of moisture transfer through the membrane on crystallization fouling in the LAMEE. The evaporation rate through the membrane is hereby adjusted by varying the relative humidity of air which changes the potential for moisture transfer between the liquid and air. Although the rate of moisture transfer through a membrane can also be adjusted by changing the solution temperature, this approach is not considered because it will alter the kinetics of the crystallization process.

A comparison of the resistance and moisture transfer flux of the LAMEE at 10% RH vs 20% RH of air is shown in Fig. 8.

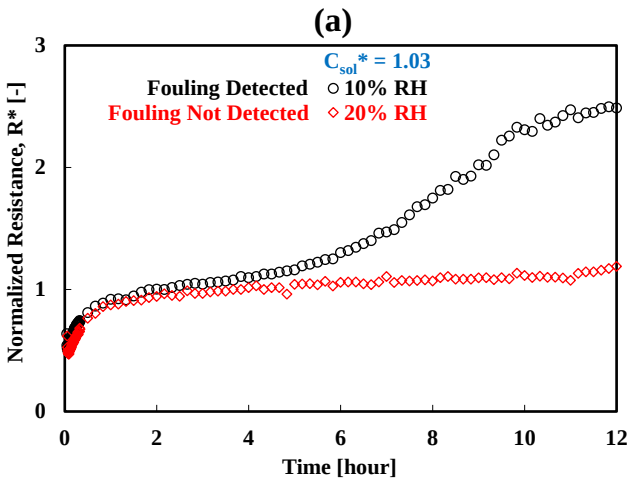

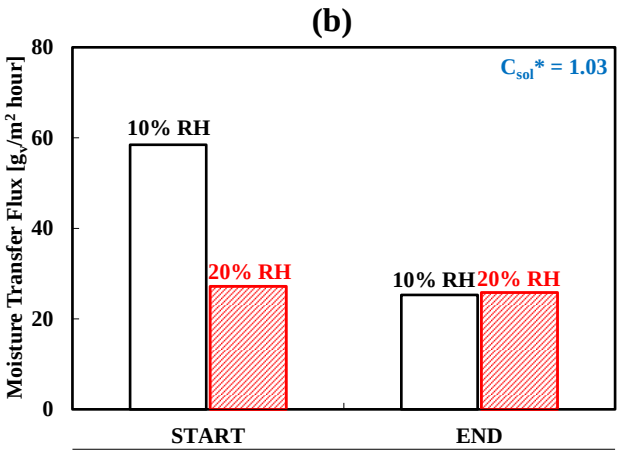

Fig. 8 Comparison of (a) normalized resistance and (b) moisture transfer flux for tests with $MgCl_2$(aq) at 10% RH vs 20% RH of air and C_{sol}* = 1.03.

Fig. 8(a) shows that the resistance of the LAMEE increases up to ~1.2 and ~2.5 for the tests with supersaturated $MgCl_2$ at 10% RH and 20% RH, respectively. Furthermore, fouling is detected for the test at 10% RH but not detected for the test at 20% RH. A possible explanation for the difference between the tests at 10% RH versus 20% RH is shown in Fig. 8(b).

Although the tests at 10% RH and 20% RH are performed with the same supersaturated solution, the moisture transfer flux at the start of the test is twice higher for 10% RH compared to 20% RH (Fig. 8b). Thus, it is possible that the higher evaporation rate for the test at 10% RH may have instigated the rapid seeding of crystals at the membrane interface, thereby leading to the accumulation of crystals which significantly increase the resistance of the LAMEE (Fig. 8a).

Furthermore, the higher evaporation rate at 10% RH may have instigated membrane fouling to such an extent that the moisture transfer flux reduces to the same value as the 20% RH test at the end of the test (Fig. 8b). Consequently, it can be concluded that the reduction in the rate of moisture transfer through the membrane for the test at 20% RH lowered the rate of crystallization fouling in the LAMEE. This implies that the LAMEE should not be operated at conditions that lead to high evaporation rates, because of the possibility of initiating crystallization fouling.

CONCLUSIONS

The key findings from this paper are outlined as follows:

1. Fouling can be detected in a LAMEE using a statistical method implemented. Fouling was detected in less than 5 hours using a supersaturated $MgCl_2$(aq) solution.
2. Crystallization fouling was found to increase the moisture transfer resistance of a LAMEE by over a factor of 2. Furthermore, linear and asymptotic fouling stages were observed.
3. The rate of crystallization fouling in a LAMEE can be lowered by reducing the rate of moisture transfer through the membrane.

ISBN: 978-0-9984188-0-3; Published online www.heatexchanger-fouling.com

NOMENCLATURE

A_{mem} Membrane surface area, m^2
C Concentration, $kg_{salt}/kg_{solution}$
h Enthalpy, J/kg
h_{fg} Latent heat of vaporization, J/kg
m Mass, kg
$\dot{m}$ Mass flow rate, kg/s
$\dot{m}''_v$ Moisture transfer flux, $g_v/m^2 \cdot hour$
q Energy, J
R Resistance, m^2 s/kg_a
t Time, s
W Humidity ratio, kg_v/kg_a

Greek Letter

σ Standard deviation

Subscript/Superscript

air Air
f Final
i Initial
in Inlet
out Outlet
sol Solution, liquid
v Water vapor
* Normalized

REFERENCES

ASME/ANSI, 1998, Performance Test Code 19.1, Test Uncertainty: Instruments and Apparatus, New York, NY.

Bansal B., Chen X. D., Müller-Steinhagen H., 2008, Analysis of "classical" deposition rate law for crystallisation fouling, *Chemical Engineering and Processing: Process Intensification,* Vol. 47, (8), pp. 1201–10.

Beriault D. E., 2011, *Run-around membrane energy exchanger prototype 4 design and laboratory testing*, University of Saskatchewan.

Bott T. R., 1997, Aspects of crystallization fouling, *Experimental Thermal and Fluid Science,* Vol. 14, (4), pp. 356–60.

Charles N. T., Johnson D. W., 2008, The occurrence and characterization of fouling during membrane evaporative cooling, *Journal of Membrane Science*, Vol. 319, (1–2), pp. 44–53.

Crawford R., da Silva A. K., 2014, Experimental testing of a passive, evaporation-based roof cooling system, *Energy Buildings,* Vol. 71, pp. 12–19.

Field R., 2010, Fundamentals of Fouling, In *Membrane Technology*, Vol. 4, pp. 1–23.

Figliola R. S., Beasley D. E., 2006, *Theory and Design for Mechanical Measurements*, Hoboken, NJ: John Wiley & Sons, Inc., 4th Ed.

Geddert T., Augustin W., Scholl S., 2011, Induction Time in Crystallization Fouling on Heat Transfer Surfaces, *Chemical Engineering Technology,* Vol. 34, (8), pp. 1303–10.

Guo W., Ngo H. H., Li J., 2012, A mini-review on membrane fouling, *Bioresource Technology,* Vol. 122, pp. 27–34.

Kim M., Park B., Lee Y. J., Lim J. L., Lee S., Kim S., 2016, Corrected normalized permeate flux for a statistics-based fouling detection method in seawater reverse osmosis process, *Desalination and Water Treatment,* Vol. 57, (51), pp. 24574–82.

Müller-Steinhagen H., 2011, Heat transfer fouling: 50 years after the Kern and Seaton model, *Heat Transfer Engineering,* Vol. 32, (1), pp. 1–13.

Mullin J. W., 2001, *Crystallization*, Oxford: Reed Educational and Professional Publishing Ltd., 4th Ed.

National Resources Canada, 2015, Energy Fact Book 2015-2016.

Pääkkönen T. M., Riihimäki M., Simonson C. J., Muurinen E., Keiski R. L., 2012, Crystallization fouling of $CaCO_3$ - Analysis of experimental thermal resistance and its uncertainty, *International Journal of Heat and Mass Transfer,* Vol. 55, (23-24), pp. 6927–37.

Pérez-Lombard L., Ortiz J., Pout C., 2008, A review on buildings energy consumption information, *Energy Buildings,* Vol. 40, (3), pp. 394–98.

Shen C., Cirone C., Jacobi A. M., Wang X., 2015, Fouling of enhanced tubes for condensers used in cooling tower systems: A literature review, *Applied Thermal Engineering,* Vol. 79, pp. 74–87.

Stamatis D. H., 2012, *Essential Statistical Concepts for the Quality Professional*, Boca Raton, FL, CRC Press.

The World Bank Group, 2016, *GDP (current US$) - Canada*, http://data.worldbank.org/indicator/NY.GDP.MKTP.CD?locations=CA.

Tijing L. D., Woo Y. C., Choi J. S., Lee S., Kim S. H., Shon H. K., 2015, Fouling and its control in membrane distillation - A review, *Journal of Membrane Science,* Vol. 475, pp. 215–44.

Walker P., Sheikholeslami R., 2003, Assessment of the effect of velocity and residence time in $CaSO_4$ precipitating flow reaction, *Chemical Engineering Science,* Vol. 58, (16), pp. 3807–16.

Woods J., 2014, Membrane processes for heating, ventilation, and air conditioning, *Renewable Sustainable Energy Reviews*, Vol. 33, pp. 290–304.

Wright S., Andrews G., Sabir H., 2009, A review of heat exchanger fouling in the context of aircraft air-conditioning systems, and the potential for electrostatic filtering, *Applied Thermal Engineering,* Vol. 29, (13), pp. 2596–2609.

Yu B. F., Hu Z. B., Liu M., Yang H. L., Kong Q. X., Liu Y. H., 2009, Review of research on air-conditioning systems and indoor air quality control for human health, *International Journal of Refrigeration,* Vol. 32, (1), pp. 3–20.

Zaytsev I. D., Aseyev G. G., 1992, *Properties of Aqueous Solutions of Electrolytes*, Boca Raton, FL, CRC Press.